Microsystem Technologies (2019) 25:4721–4730
https://doi.org/10.1007/s00542-019-04513-0

TECHNICAL PAPER

Low envelope correlation coefficient, enhanced gain, and suppressed mutual coupling in compact 4-port MIMO microstrip antenna loaded with metasurface

Aashish Kumar[1] · C. S. Rai[1] · Mukesh Kumar Khandelwal[2] · Binod Kumar Kanaujia[3]

Received: 4 March 2019 / Accepted: 31 May 2019 / Published online: 8 June 2019

Abstract
Four port MIMO microstrip antenna is proposed for C-band wireless applications. Proposed antenna is embedded with metasurface after achieving the compactness of 17.25%. Analysis of metasurface including double negative characteristics, dispersion curve, and zeroth order frequency is presented. Furthermore, techniques for suppression of mutual coupling, suppression of cross-polarization, and enhancement of antenna gain are also described. Moreover, proposed antenna is fabricated and simulated results are validated through experimental results of fabricated prototypes.

1 Introduction

Antenna is an essential component of any wireless system because no signal can be transmitted wirelessly from any system without having an antenna. Microstrip antennas have become the first choice of researchers now-a-days for single-chip devices. Compact antennas which can be used for than one device/system are in demand now-a-days. For the same, multi input and multi output (MIMO) antennas are popular because of their ability to transmit or receive the signals from more than one device simultaneously. Various MIMO antennas have been proposed for different wireless applications (Saxena et al. 2017, 2018). Two-port MIMO antenna has been proposed with polarization diversity for ultrawide band (UWB) applications (Saxena et al. 2017).

Suppression of mutual coupling between different ports of MIMO antenna is the main challenge for researchers. Several works have been reported for the suppression of mutual coupling of MIMO antennas (Saxena et al. 2017, 2018; Jha and Sharma 2018; Khandelwal et al. 2018a). In Saxena et al. (2018); a built-in circular isolator was embedded within the structure of two-port MIMO antenna to suppress the mutual coupling between both ports. Whereas in Jha and Sharma (2018), a quasi-elliptical planar monopole antenna was proposed with minimum mutual coupling. Defected Ground Structure (DGS) also has been used to reduce the amount of mutual coupling in two-port antenna as demonstrated in Khandelwal et al. (2018a). Envelope correlation coefficient (ECC) is the factor for scaling the mutual coupling among multiple ports of MIMO antenna (Jha and Sharma 2018).

When a microstrip antenna is operated in its fundamental mode, its major radiations are polarized in a principle plane and referred as co-polarized radiations (CP) however few radiations are also polarized in the orthogonal plane to the principle plane which degrade the radiation properties of that antenna and known as cross-polar radiations (XP) (Ludwig 1973; Lee et al. 1992). XP radiations below the value of − 20 dB and proper isolation between CP and XP radiations are the most desirable requirements of an efficient system. Many researchers have reported their research work for the suppression of XP radiations

✉ Mukesh Kumar Khandelwal
mukesh.khandelwal89@ieee.org

Aashish Kumar
ashish.mogha01@gmail.com

C. S. Rai
csrai@ipu.ac.in

Binod Kumar Kanaujia
bkkanaujia@yahoo.co.in

[1] School of Information and Communication Technology, Guru Gobind Singh Indraprastha University, Delhi, India

[2] Department of Electronics and Communication Engineering, Bhagwan Parshuram Institute of Technology, Delhi 110089, India

[3] Department of Computational and Integrative Sciences, Jawaharlal Nehru University, Delhi 110067, India

and the enhancement of isolation level between CP and XP radiations (Khandelwal et al. 2014a, b, 2015, 2016, 2018a; Keshri et al. 2017; Sharma et al. 2018). XP radiations are defined properly in (Ludwig 1973) on the other hand these radiations were studied for the conventional circular patch antenna in (Lee et al. 1992) which gave the understanding aspects of XP radiations of a microstrip patch antenna structure. In (Khandelwal et al. 2014a, b, 2015, 2016, 2018a; Keshri et al. 2017; Sharma et al. 2018), it is noticed that DGS is the most suitable and widely used technique for the suppression of XP radiations (Khandelwal et al. 2014a, b, 2015, 2016, 2018a; Keshri et al. 2017; Sharma et al. 2018). Arc shaped DGS has been used to reduce the amount of mutual coupling as well as XP radiations (Khandelwal et al. 2018a). Circular DGS was used underneath the open end of the microstrip line in single (Khandelwal et al. 2014) and double layer (Khandelwal et al. 2015) microstrip antennas to reduce the XP

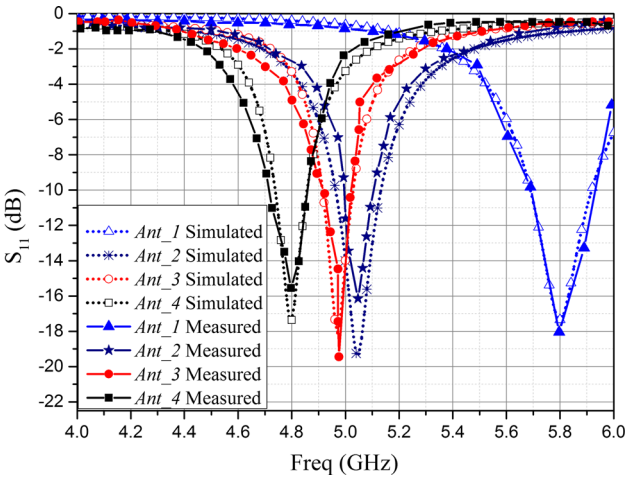

Fig. 3 Simulated and measured S_{11} variation with frequency of *Ant_1*, *Ant_2*, *Ant_3*, and *Ant_4*

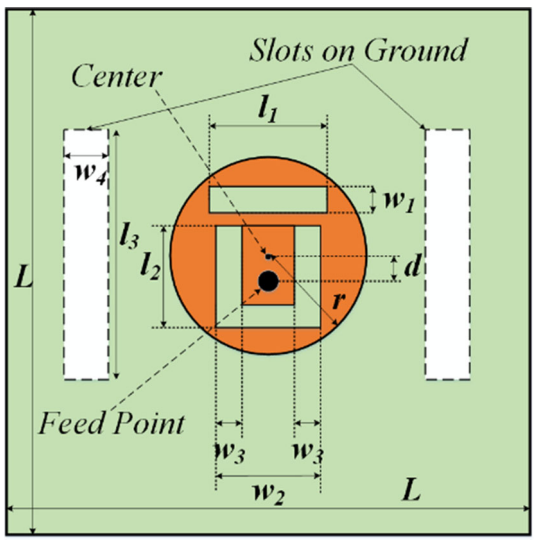

Fig. 1 Schematic of proposed antenna

radiations. Random shaped DGS also have been used to reduce the XP radiations in UWB (Khandelwal et al. 2014) and triple band antennas (Khandelwal et al. 2016). Moreover, DGS has been used to suppress the XP radiations of omnidirectional microstrip antenna (Keshri et al. 2017). In Sharma et al. (2018), DGS was introduced to enhance the gain and to suppress the XP radiations of four element antenna array.

In the earlier studies, the focus was mainly on the suppression of the XP radiations. In order to overcome the shortcomings of the previous studies (Khandelwal et al. 2014a, b, 2015, 2016, 2018a; Ludwig 1973; Lee et al. 1992; Keshri et al. 2017; Sharma et al. 2018), new geometry of defects in the ground plane with improved performance is proposed in the present communication which not only suppress the XP level of antenna but also improves the mutual coupling of MIMO antenna.

In this work, a slotted circular microstrip patch antenna (CMPA) is proposed with DGS for C-band wireless applications. C-Band contains a very wide range of

(a) **(b)**

Fig. 2 Photographs of the prototype: **a** top view of *Ant_4*, **b** bottom view of ground plane

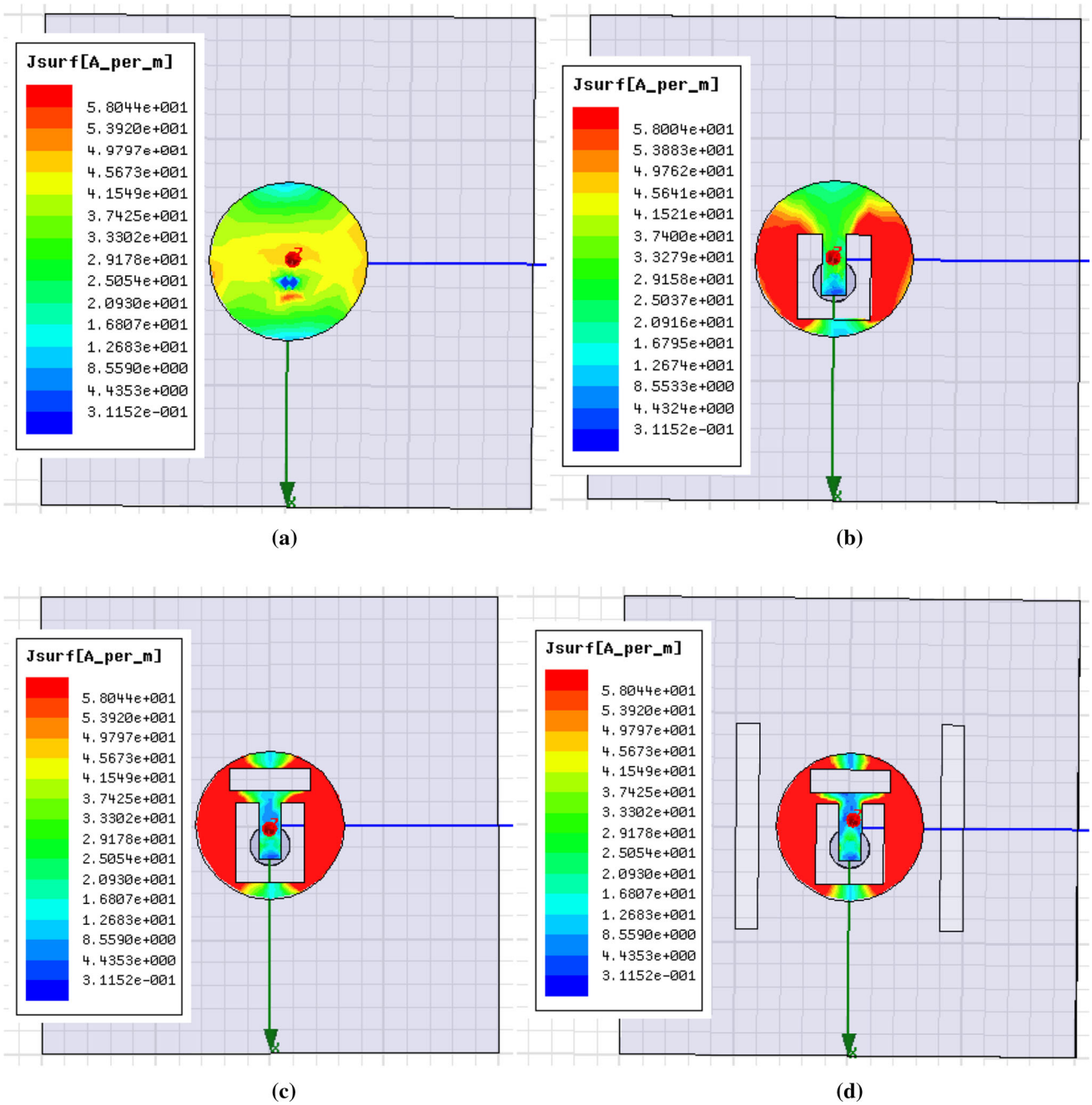

Fig. 4 Current distribution of **a** *Ant_1* at 5.8 GHz, **b** *Ant_2* at 5.05 GHz, **c** *Ant_3* at 4.97 GHz, and **d** *Ant_4* at 4.8 GHz

applications including satellite communication transmission, surveillance radar, whether radar, cordless telephones and some WiFi systems. The functionality of proposed CMPA is further enhanced by introducing a rectangular slot along with U-slot in the circular patch which improves the compactness of the structure. XP radiations of the structure are suppressed by embedding the array of rectangular slots in the ground plane. Then, 4-port MIMO antenna is designed and its mutual coupling is suppressed further through DGS. Furthermore, a metasurface is designed and its analysis is presented. Double negative characteristics, dispersion curve and zeroth order frequency (ZOR) of metasurface are analyzed. Then, designed metasurface is embedded with proposed antenna to enhance the antenna gain. The analysis is carried out by finite element method (FEM) using Ansoft HFSS v.15. The simulated results are verified by measured results of fabricated prototypes.

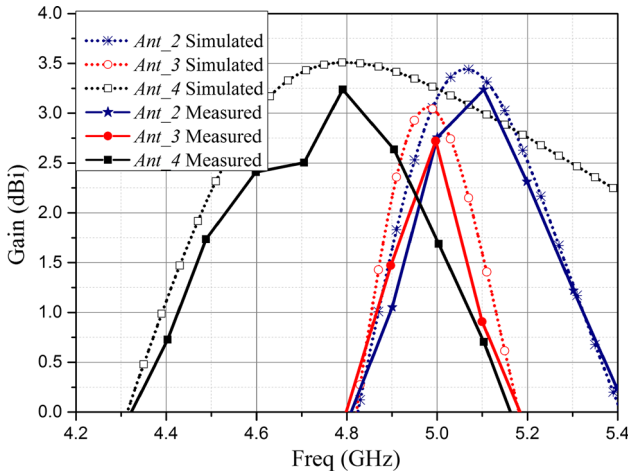

Fig. 5 Simulated and measured antenna gain variation with frequency of *Ant_1*, *Ant_2*, *Ant_3*, and *Ant_4*

2 Antenna geometry

The schematic of the proposed structure is shown in Fig. 1. A microstrip circular patch antenna of radius r supported by a regular ground plane is used as reference antenna and same is referred as *Ant_1* in present study. Radius r of circular patch is calculated as 6.5 mm corresponding to 5.8 GHz frequency (Balanis 1997). A 50 Ω coaxial feed is provided through SMA connector at a distance d = 1.81 mm from the center of patch. Further, a U-shaped slot and a rectangular slot of dimensions $l_1 \times w_1$ are embedded in the circular patch. After integrating these slots, resonant frequency is shifted towards its left (lower value), which implies for the compactness of antenna. The current path on the circular patch is increased (current starts to flow around the periphery of the slots) and results in the increased electrical length (lamda) corresponding to lower frequency. The dimensions of the U-slot are determined by its length l_2, width w_2, and thickness w_3. The values of l_2, w_2 and w_3 are taken as 7 mm, 6 mm and 2 mm respectively. Only U-slot loaded circular microstrip patch antenna with regular ground plane is referred as *Ant_2* whereas antenna with both slots (U as well as rectangular slot) is referred as *Ant_3*. The length l_1 and width w_1 of rectangular slot is taken as 7 mm and 2 mm, respectively. Furthermore, two identical rectangular slots are embedded symmetrically in the ground plane which results in the suppressed XP radiations. The dimensions of the defects are determined by its length l_3 and width w_4 and location b. The values of length l_3 and width w_4 are chosen as 18 mm and 2 mm, respectively. The location b is taken in such a way that the distance between inner boundaries of the both defects should be 8 mm apart from the center of the patch. This proposed structure with rectangular DGS is referred as *Ant_4* for this study. Figure 2 shows the photograph of the fabricated prototypes of the proposed antenna.

3 Single port antenna

Proposed antenna is designed on FR-4 epoxy substrate of thickness h = 1.6 mm and dimensions of 40 mm × 40 mm with dielectric constant ε_r= 4.4 and loss tangent tanδ = 0.02. Fabrication is done by standard photolithography process and measurement of fabricated antennas is done on Agilent Vector Network Analyzer (VNA) N5230A and Agilent Spectrum Analyzer in anechoic chamber. Figure 3 shows the simulated and measured S_{11} variation with frequency of *Ant_1*, *Ant_2*, *Ant_3*, and *Ant_4*. It is observed from Fig. 3 that reference antenna *Ant_1* is resonating at 5.8 GHz.

Current path (electrical length) is increased by embedding the U-shaped slot on the circular patch thus 12.93% of compactness is achieved in *Ant_2* and it starts to resonate at 5.05 GHz. Compactness is further improved to the value of 14.31% by embedding a rectangular slot along with U-shaped slot on the circular patch in the case of *Ant_3* and it starts to resonates at 4.97 GHz. Further, two rectangular defects are introduced on the ground plane of the proposed structure and response is achieved at 4.8 GHz with further compactness of 17.25% as shown in Fig. 3.

Current distributions of all the four proposed antennas are shown in Fig. 4 at their respective resonant frequencies. It is clear from the Fig. 4, slots are contributing to improve the radiation characteristics of the proposed antennas. It is observed that current is concentrated around the slots and results in increased current patch which is responsible for miniaturization. When a slot is introduced on a conducting surface, current is started to flow around the periphery of that slot thus total electrical length (length covered by wave) is increased. Increased electrical length corresponding to the decreased (lower) frequency represents the miniaturization. After observing the current distribution of proposed structures at different frequencies it is concluded that antennas are showing better characteristics only at their respective resonant frequencies. At other than the resonant frequencies antennas are not showing satisfactory results.

Figure 5 shows the simulated and measured gain characteristics of all the proposed antennas. *Ant_2*, *Ant_3* and *Ant_4* show their peak gain of the values of 3.49, 3.1 and 3.501 dBi at their respective resonant frequencies 5.05, 4.97, and 4.8 GHz, respectively. Measured results of gain of fabricated antennas are in good agreement with simulated results of the proposed antennas.

Figures 6 and 7 show the radiation characteristics of the proposed antennas. The simulated and measured polar

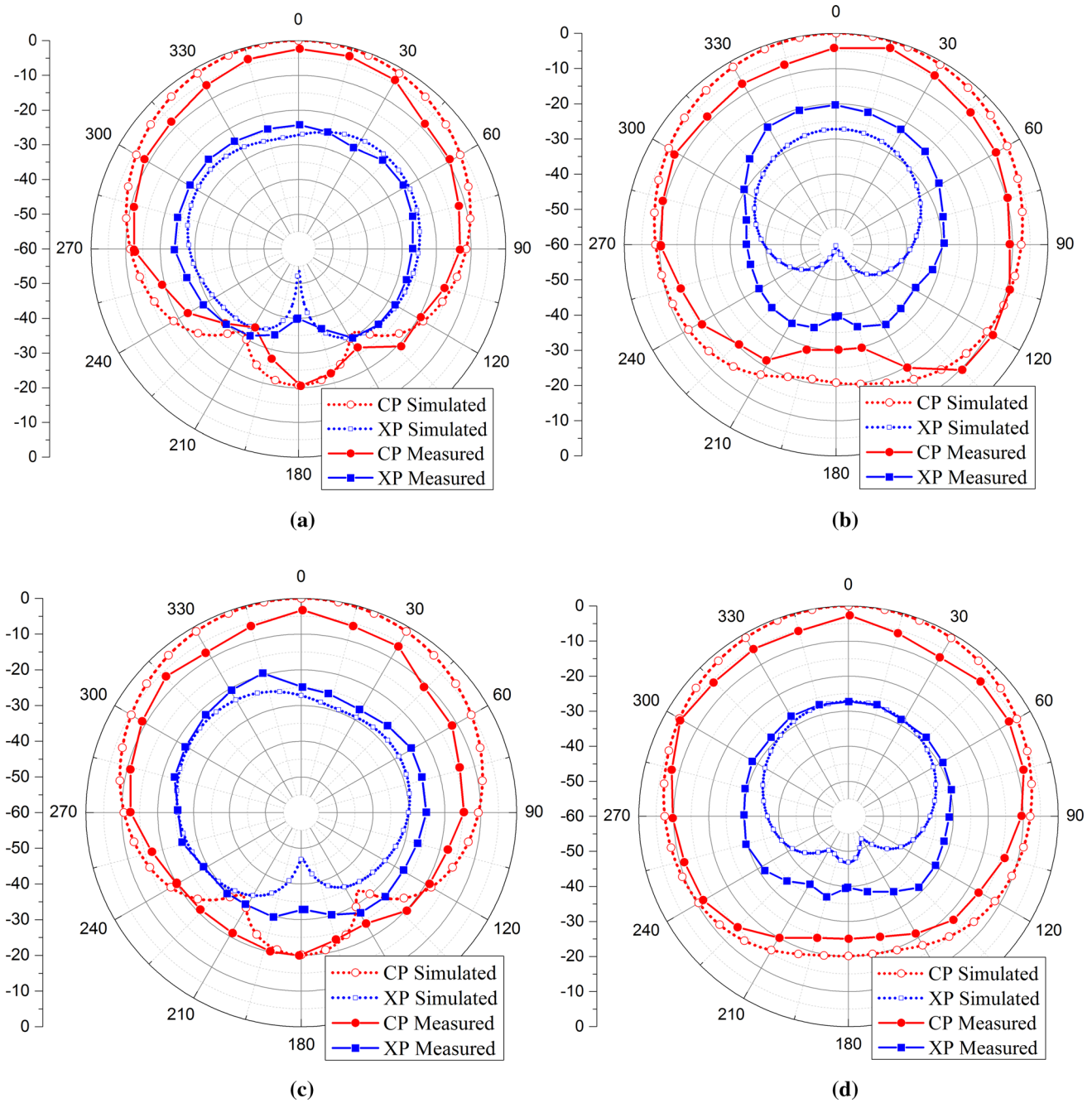

Fig. 6 Normalized radiation pattern of **a** E-plane of *Ant_1* at 5.8 GHz, **b** H-plane of *Ant_1* at 5.8 GHz, **c** E-plane of *Ant_2* at 5.05 GHz, **d** H-plane of *Ant_2* at 5.05 GHz, **e** E-plane of *Ant_3* at 4.97 GHz, **f** H-plane of *Ant_3* at 4.97 GHz, **g** E-plane of *Ant_4* at 4.8 GHz, and **h** H-plane of *Ant_4* at 4.8 GHz

radiation pattern of CP and XP in both major orthogonal *E* and *H* planes are shown in Fig. 6 whereas a comparison of simulated radiation pattern in both *E* and *H* planes of all the antennas at their respective resonance frequencies in rectangular format is presented in Fig. 7a, b, respectively. It is observed that CP characteristics are almost same of all antennas in both *E* and *H* planes. Cross-polarization level of *Ant_4* is lowest among all the antennas and about 8 dB of suppression is obtained in comparison with other antennas. XP level of *Ant_4* is maintained below 28 dB and 36 dB in *E* and *H* planes, respectively.

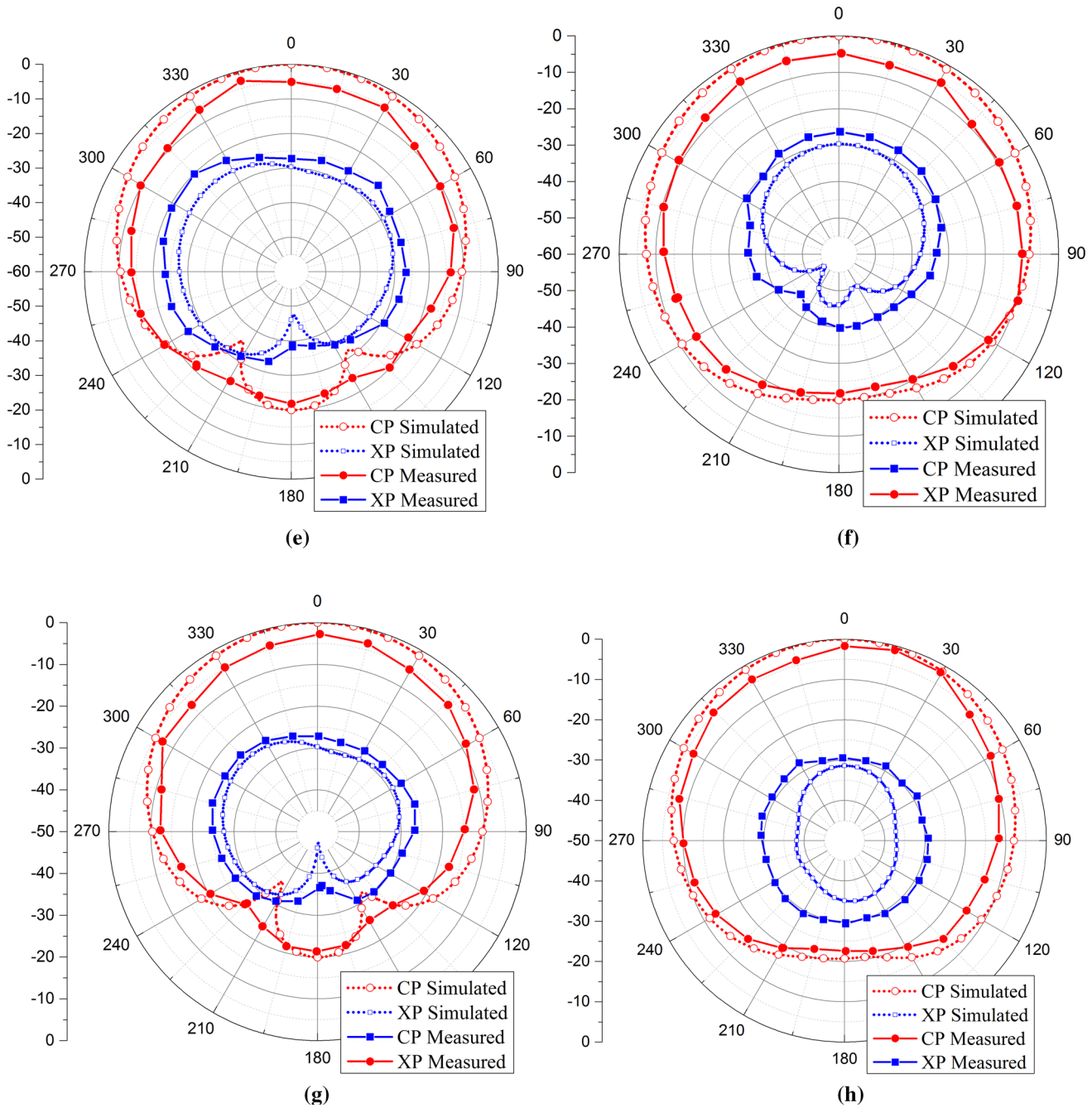

Fig. 6 continued

4 Analysis of MIMO antenna

Further, four element MIMO antenna is designed with four ports. Each element is spaced at quarter wavelength to each other and port numbers are assigned as shown in Fig. 8. Vertical rectangular defects contribute to suppress the mutual coupling between port#1 and port#2, port#3 and port#4 and vice versa. A horizontal rectangular slot is embedded in the ground plane which minimize the mutual coupling between port#1 and port#4, port#2 and port#3, port#1 and port#3, port#2 and port#4 and vice versa respectively. Defects in the ground plane perturbs the surface waves which are moving from one port to another port and results in suppressed mutual coupling. Return loss characteristics of individual port remain same as shown in Fig. 3 for *Ant_4*. Mutual coupling among all the four ports are shown in Fig. 9 through S-parameters.

Moreover, a metallic reflector and a metasurface is embedded with proposed MIMO antenna to enhance its radiation characteristics as shown in Fig. 10. A metallic

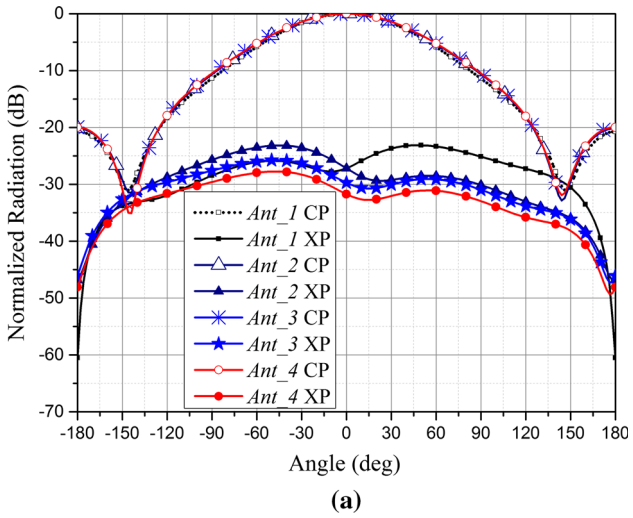

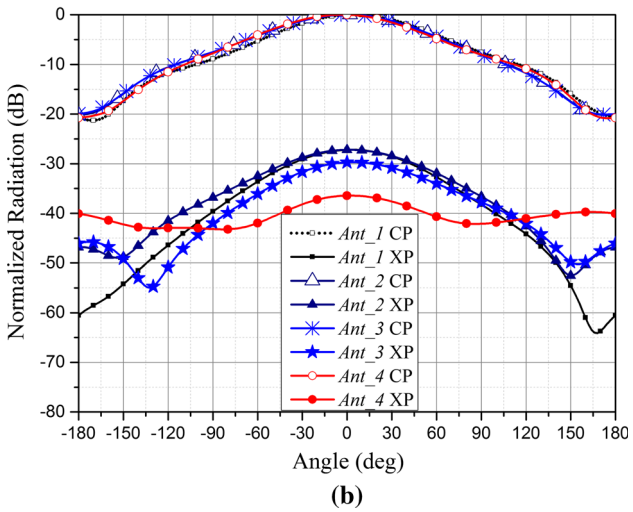

Fig. 7 Comparison of simulated co-polar and cross-polar radiations in **a** E-plane, and **b** H-plane

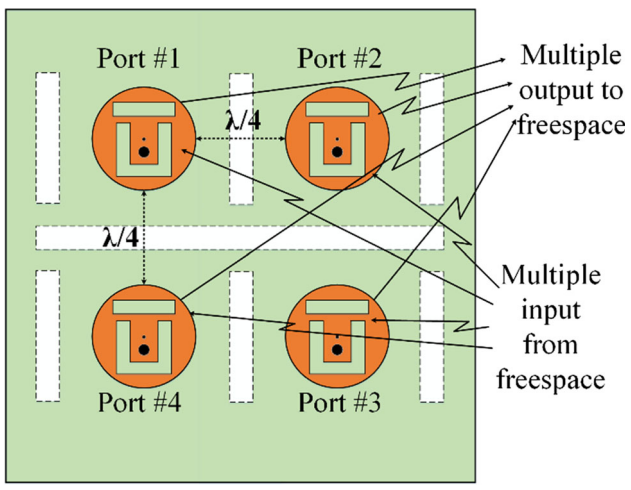

Fig. 8 Schematic of 4-port MIMO antenna

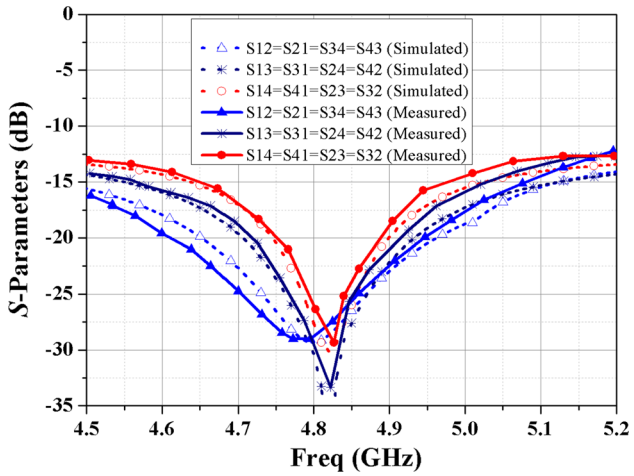

Fig. 9 Simulated and measured *S*-parameters of 4-port MIMO antenna

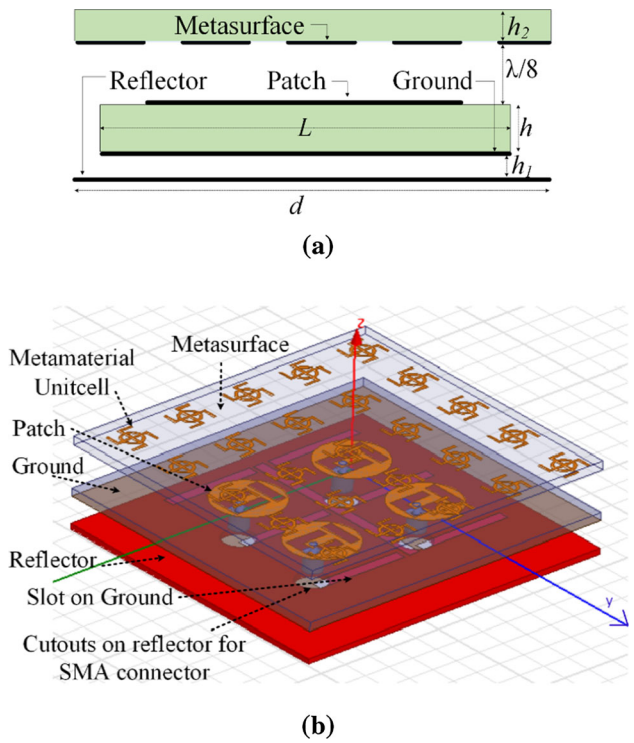

Fig. 10 Schematic of proposed antenna with metallic reflector and metasurface, **a** side view, **b** prototype

plate of 1 mm thickness is used as a reflector below the lower surface of the MIMO antenna at a distance h_1= 3 mm. This metallic reflector reflects back the backward radiations in forward direction which contribute to enhance the gain of the structure. Proposed metallic reflector has four circular cutouts for connecting the probes to SMA connector and four cylindrical Teflon rods are used at all four corners of this metallic reflector to support the MIMO antenna. The effects of metallic reflector-height h_1

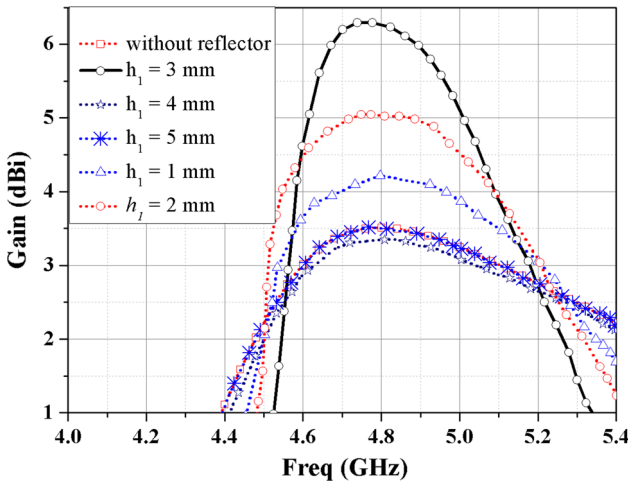

Fig. 11 Simulated gain variations for different values of reflector distance h_1 when metasurface is not embedded with structure

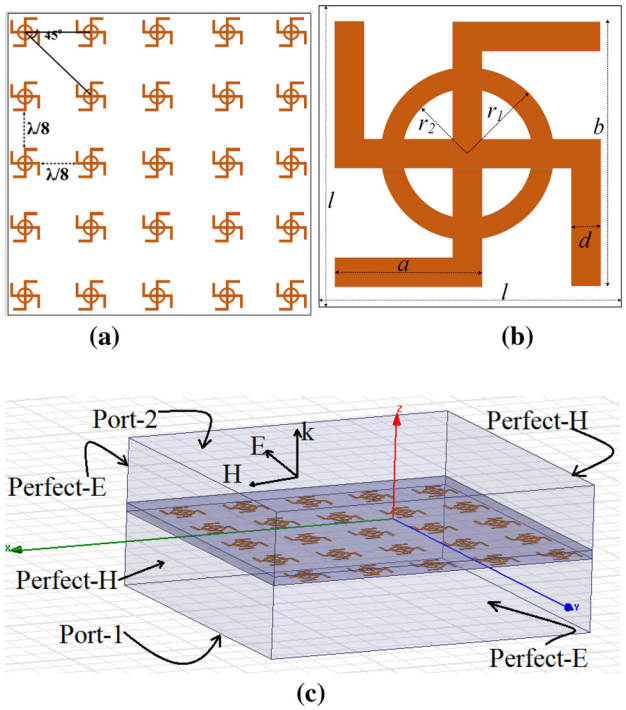

Fig. 12 Schematic of metasurface, **a** metasurface, **b** unit cell, **c** analysis setup in HFSS

on antenna gain is shown in Fig. 11. At the height of 3 mm, best results are obtained. Approximately, same results are obtained above 3 mm distance.

Further, a metasurface of same outer dimensions is placed at λ/8 height above the upper surface of the antenna. An array of 5 × 5 of unit cell is placed on the lower surface of FR-4 epoxy substrate of thickness h_2 = 0.8 mm. Unit cells are spaced at diagonal angle of 45° and λ/8 distance to each other.

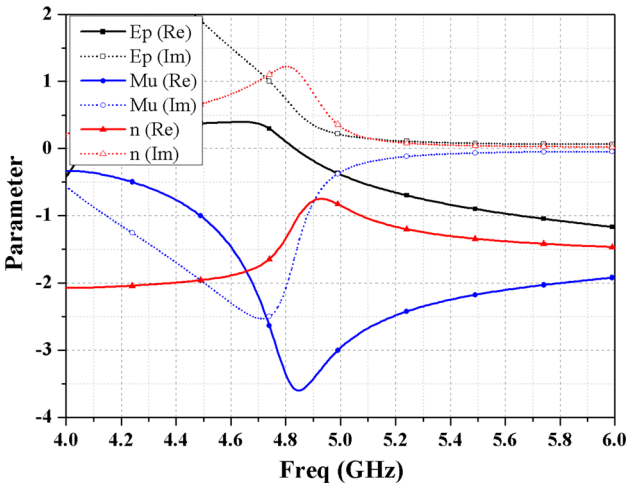

Fig. 13 Simulated results of metasurface; effective permeability, permittivity and refractive index

Fig. 14 Dispersion diagram of proposed metasurface

Schematic of metasurface and unit cell is shown in Fig. 12a, b respectively. Analysis setup for metasurface in HFSS is depicted in Fig. 12c. Metasurface is analyzed in waveguide environment for which left and back surfaces are assigned as perfect-H whereas front and back surfaces are assigned as perfect-E. Port_1 and Port_2 are considered on lower and upper face of the waveguide. Magnitude and phase of the S-parameters are extracted from HFSS and their complex values are calculated and referred as S_{11_c} and S_{12_c}. The impedance Z of the structure is calculated as (Khandelwal et al. 2017, 2018b)

$$Z = \pm\sqrt{\frac{(1+S_{11_c})^2 - S_{12\_c}{}^2}{(1-S_{11_c})^2 - S_{12\_c}{}^2}} \quad (1)$$

where S_{11_c} and S_{12_c} are the complex S-parameters and expressed as

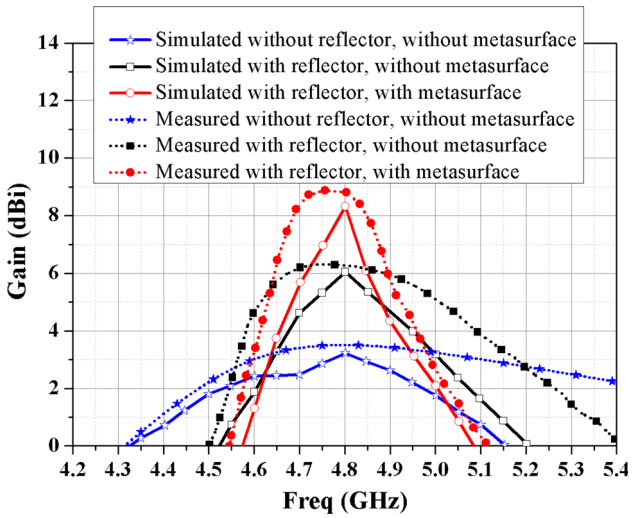

Fig. 15 Simulated and measured gain of proposed antenna with and without reflector and metasurface

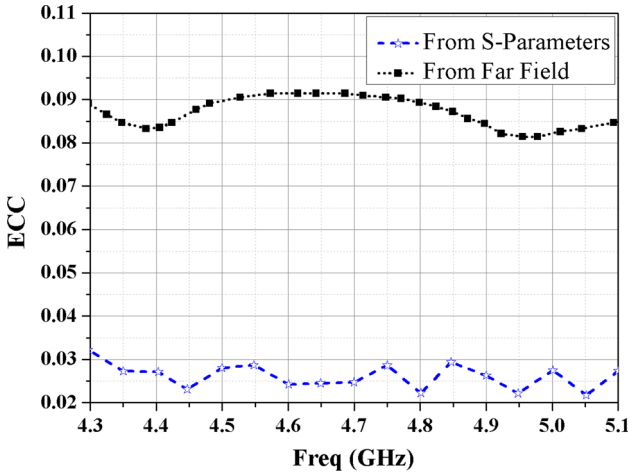

Fig. 16 ECC of proposed MIMO antenna

$$S_{11\_c} = S_{11\_m} \times \left\{\cos\left(S_{11\_p}\right) + j.\sin\left(S_{11\_p}\right)\right\} \quad (2)$$

$$S_{12\_c} = S_{12_m} \times \left\{\cos\left(S_{12_p}\right) + j.\sin\left(S_{12_p}\right)\right\} \quad (3)$$

where S_{11_m} and S_{11_p} are the magnitude and phase of the *S*-parameters of the metasurface and obtained from HFSS.

The refractive index n is calculated from Eq. 4

$$e^{jnk_0 l} = \frac{S_{12\_c}}{1 - S_{11\_c}\frac{Z-1}{Z+1}} \quad (4)$$

where k_0 is the wave number in the free space and l is the largest dimension of the unit cell.

The effective permittivity E_p and effective permeability M_u are calculated as

$$E_p = \frac{n}{Z}, M_u = nZ \quad (5)$$

Effective permittivity, effective permeability and refractive index is shown in Fig. 13 and it is observed that at antenna resonant frequency 4.8 GHz, proposed metasurface shows double negative (DNG) characteristics. Thus, metasurface affects the field radiated by antenna at 4.8 GHz. Dispersion diagram of the metasurface is depicted in Fig. 14 and zeroth order resonance (ZOR) frequency is observed at 4.8 GHz as the value of dispersion coefficient beta (β) is zero at 4.8 GHz. Left-handed and right-handed regions can be visualized by the ZOR frequency at dispersion diagram.

Figure 15 shows the simulated and measured gain of proposed antenna with and without metasurface and reflector. Gain of about 8.8 dBi is achieved when metasurface is placed at the height of λ/8. Metallic reflector and metasurface are placed in the near-reactive region of the antenna thus they perturbed the field radiated from the antenna and contribute in enhanced gain. ECC of MIMO antenna is shown in Fig. 16 which can be obtained from Jha and Sharma (2018). ECC should be less than 0.5 for MIMO antenna which shows that multiple elements of MIMO antenna have minimum overlapping region and better isolation (Jha and Sharma 2018). A comparative study of all the four antennas are given in Table 1. Prototypes of proposed fabricated antennas are demonstrated in Fig. 17.

5 Conclusion

Compact microstrip antenna with suppressed cross-polarization level is designed, analyzed and fabricated. 17.25% of miniaturization is achieved by the proposed technique with better radiation characteristics. Proposed antenna

Table 1 Comparative analysis of the proposed antennas

Structure name	Resonant frequency (GHz)	Compactness (%)	S11 (dB)	Gain (dBi)	E-plane XP level (dB)	H-plane XP level (dB)
Ant_1	5.8	–	− 18	3.4	− 21	− 28
Ant_2	5.05	12.93	− 19.5	3.49	− 21	− 28
Ant_3	4.97	14.31	− 19.6	3.1	− 26	− 32
Ant_4	4.8	17.25	− 17.9	3.501	− 28	− 36

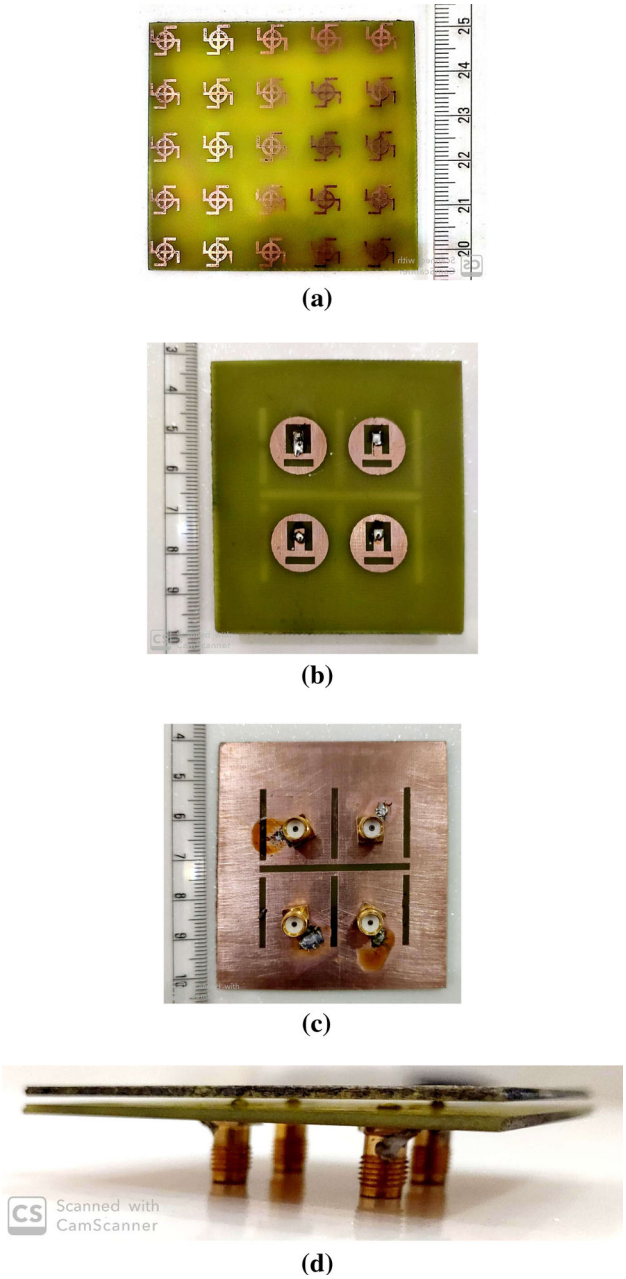

Fig. 17 Fabricated prototypes of proposed **a** metasurface, **b** top view of 4-port antenna without stacking, **c** bottom view of 4-port antenna without stacking, **d** side view of proposed antenna

shows satisfactory gain within operating band and maintained cross polarization level below 28 dB and 36 dB in *E* and *H* planes respectively. Further, 4-port MIMO antenna is designed and analyzed which is further embedded with metallic reflector and metasurface for enhancing the antenna gain. Design and analysis of metasurface is also presented. DNG characteristics, dispersion curve and ZOR frequency of metasurface is analyzed and presented. ECC of 4-port MIMO antenna is achieved below the value of 0.1. The measured results of fabricated antennas are validating the simulated results successfully. The proposed antenna may be a nice candidate for wireless application in C-band with low cross-polarized radiation level.

References

Balanis CA (1997) Antenna theory: analysis and design. Wiley, Noida

Jha KR, Sharma SK (2018) Combination of frequency agile and quasi-elliptical planar monopole antennas in MIMO implementations for handheld devices. IEEE Antennas Propag Mag 60(1):118–131

Keshri JP, Kanaujia BK, Khandelwal MK, Bakariya P, Mehra RM (2017) Omnidirectional multiband stacked microstrip patch antenna with wide impedance bandwidth and suppressed cross-polarization. Int J Microw Wirel Technol 9(3):629–638

Khandelwal MK, Kanaujia BK, Dwari S, Kumar S (2014a) Analysis and design of microstrip-line-fed antenna with defected ground structure for Ku band applications. Int J Electron Commun 68(10):951–957

Khandelwal MK, Kanaujia BK, Dwari S, Kumar S (2014b) Bandwidth enhancement and cross-polarization suppression in ultra-wideband microstrip antenna with defected ground plane. Microw Opt Technol Lett 56(9):2141–2146

Khandelwal MK, Kanaujia BK, Dwari S, Kumar S (2015) Analysis and design of dual band compact stacked microstrip patch antenna with defected ground structure for WLAN/WiMax applications. Int J Electron Commun 69(1):39–47

Khandelwal MK, Kanaujia BK, Dwari S, Kumar S, Gautam AK (2016) Triple band circularly polarized microstrip antenna with defected ground structure for wireless applications. Int J Microw Wirel Technol 8(6):943–953

Khandelwal MK, Kanaujia BK, Kumar S, Gautam AK (2017) Miniaturization of DNG metamaterial. Microw Opt Technol Lett 59(4):862–865

Khandelwal MK, Kumar S, Kanaujia BK (2018a) Design, modeling and analysis of dual feed defected ground microstrip patch antenna with wide axial ratio bandwidth. J Comput Electron 17(3):1019–1028

Khandelwal MK, Arora A, Kumar S, Kim KW, Choi HC (2018b) Dual band double negative (DNG) metamaterial with small frequency ratio. J Electromagn Waves Appl. https://doi.org/10.1080/09205071.2018.1498026

Lee KF, Luk KM, Tam PY (1992) Cross-polarization characteristics of circular patch antenna. Electron Lett 28(6):587–589

Ludwig AC (1973) The definition of cross polarization. IEEE Trans Antennas Propag 21(1):116–119

Saxena S, Kanaujia BK, Dwari S, Kumar S, Tiwari R (2017) A compact dual polarized MIMO antenna with distinct diversity performance for UWB applications. IEEE Antennas Wirel Propag Lett 16:3096–3099

Saxena S, Kanaujia BK, Dwari S, Kumar S, Tiwari R (2018) MIMO antenna with built-in circular shaped isolator for sub-6 GHz 5G applications. Electron Lett 54(8):478–480

Sharma S, Mainuddin, Kanaujia BK, Khandelwal MK (2018) Design of 4-element microstrip array of wideband reflector antenna with stable high gain characteristics. Microsyst Technol. https://doi.org/10.1007/s00542-018-4189-3